Voltage imaging reveals the emergence of population activity in the spinal cord

Asuka Shiraishi[1#], Ayane Hayashi[2#], Narumi Fukuda[1], Mari Hishinuma[1], Hiroaki Miyazawa[1], Sachiko Tsuda[1§]

1 Division of Life Science, Graduate School of Science and Engineering, Saitama University, 255 Shimo-Okubo, Sakura-ku, Saitama City, Saitama 338-8570, Japan

2 Department of Regulatory Biology, Faculty of Science, Saitama University, 255 Shimo-Okubo, Sakura-ku, Saitama City, Saitama 338-8570, Japan

# These authors contributed equally.

[§]Author for correspondence (stsuda@mail.saitama-u.ac.jp)

Abstract

One of the central questions in neural development is how individual neurons assemble functional networks. To address this, it is essential to elucidate how coordinated activity emerges during development. However, tracking the functional maturation of neuronal populations over time remains challenging, as it requires long-term, non-invasive monitoring of membrane potential dynamics. Here, we developed a voltage imaging approach for zebrafish embryos using genetically encoded voltage indicators (GEVIs), enabling fast, direct and cell-type-specific measurements of membrane potentials from defined neuronal populations in a non-invasive manner. Using this approach, we detected coordinated voltage changes in spinal motor neurons with high spatiotemporal resolution. Depolarization and hyperpolarization events were observed at the population, single-cell, and subcellular levels. Notably, long-term voltage imaging revealed the early emergence and progressive maturation of membrane potential dynamics, characterized by increased firing rate, coupling strength and axonal outgrowth. This optical approach constitutes a significant advancement in the study of neural development, providing a powerful tool for investigating the spatiotemporal dynamics of neuronal populations in vivo.

Introduction

The nervous system is composed of a vast number of neurons that perform diverse functions. How are these neurons generated and how do they communicate with each other to form functional networks? To better understand the function and development of the nervous system, it is crucial to examine the dynamic behavior of neuronal populations and how these dynamics evolve over time. However, such investigations are often hampered by the huge number of neurons involved and the invasiveness of conventional electrophysiological recording techniques.

Optical methods provide a powerful alternative, as light facilitates non-invasive access to large populations of neurons, which is difficult with electrophysiological recordings that insert electrodes into target tissues as single-point detectors. Voltage imaging enables fast, direct, and simultaneous detection of membrane potentials across multiple cells, providing an excellent system for understanding the dynamic behavior of neuronal populations [1-3]. Its high speed and directness allow the detection of action potentials, hyperpolarization, and subthreshold responses, which are difficult to examine using calcium imaging, partly because of the slow kinetics of the indicators and the dynamics of calcium [4, 5]. Various voltage-sensitive dyes have been developed to improve brightness, signal-to-noise ratio, and spectral range, thereby advancing our understanding of network dynamics in the brain [6-10]. More recently, genetically encoded voltage indicators (GEVIs) have been developed, allowing for cell-type-specific voltage imaging [11-13]. These GEVIs include the ones based on voltage-sensitive phosphatase domains [14-17], as well as microbial rhodopsin-based sensors [18-21]. Although GEVIs have been successfully applied to investigate brain and cardiac function [22-29], their application to developmental studies of the nervous system remains limited. This is largely due to the technical challenges of achieving long-term, non-invasive voltage imaging in developing tissues.

One of the earliest neural structures to develop is the spinal cord, which serve as the core of rhythmic motor behaviors through central pattern generators [30]. Neurons in the spinal cord, including motor neurons, exhibit prominent population activity even at early in development. This activity drives fetal movement and is suggested to play a critical role for circuit formation [31, 32]. While electrophysiological studies have characterized the firing properties of these

neurons, the spatiotemporal organization and developmental emergence of their coordinated voltage dynamics, the core of the remain to be understood [33-35].

In this study, to examine the spatiotemporal dynamics of neuronal populations and their emergence during development, we applied GEVI ArcLight to zebrafish embryos, taking advantage of their optical transparency, genetic tools, and rapid development [36, 37]. Although recent studies have employed GEVIs in zebrafish larvae primarily to explore circuit function [20, 21, 24, 25, 28], long-term developmental imaging has not yet been achieved. Here, we establish a long-term voltage imaging approach that enables the observation of voltage dynamics in neuronal populations over the course of development. This approach allowed us to reveal how coordinated voltage activity emerge during early neural development.

Materials and Methods

Fish lines

Wild-type zebrafish (Danio rerio) with RW genetic background or nacre line were used [38]. *Tg(elavl3:GAL4-VP16)*, *Tg(UAS:lynRFP)*, and *Tg(elavl3:GCaMP6f)* fish lines have been described previously and obtained from the National BioResource Project [24, 39]. The Tg lines were crossed with the nacre line. All procedures were performed in accordance with a protocol approved by the Saitama University Committee on Animal Research.

DNA Construction and establishment of ArcLight transgenic line

To generate pTol2-UAS-ArcLight plasmid, ArcLight-A242 sequence was excited from the pCS2-ArcLight-A242 plasmid (Addgene) and inserted into pTol2-UAS-MCSF-polyA, in which UAS and polyA sequences were integrated into the pTol2-MCS plasmid [40]. To establish pTol2-UAS-ArcLight line, Tol2 plasmid DNA and *transposase* mRNA were co-injected into one-cell-stage embryos. Genotyping was performed using the primers for ArcLight-A242 (5′-TCGACGGTATCGATAAGCTTGC-3′,5′- CACCTCCCCCTGAACCTGAAACATA-3′).

Transient expression of ArcLight in the spinal cord and cerebellum

For the spinal cord, 25 ng/μl pTol2-UAS-ArcLight-A242-polyA plasmid DNA was co-

injected with 25 ng/μl *Tol2 transposase* mRNA into one-cell-stage embryos of *Tg(elavl3:GAL4-VP16)* embryos, which express Gal4 in neurons [39]. After the injection, the embryos were incubated at 23°C and then transferred to 28°C by 18 hour post fertilization (hpf). ArcLight-positive embryos were screened at the 18.5 to 19 hpf, followed by voltage imaging.

Confocal imaging

Zebrafish embryos were paralyzed in 0.02% tricaine and mounted on 2% low melting-point agarose (Sigma-Aldrich). Optical sectioning was performed using an Olympus FV1000 or a Nikon A1R confocal microscope. ImageJ, NIS-Elements (Nikon), and Imaris (Bitplane) programs were used to perform the image analysis.

Voltage imaging

Embryos from 16 to 23 hpf were paralyzed with tubocurarine (0.5 mM, Sigma-Aldrich), with their tail tips cut for better penetration of tubocurarine [41, 42]. Then, embryos were mounted on 1.8% low melting-point agarose containing 0.1-0.2 mM tubocurarine. After embedding the embryos onto 1% agarose, an extracellular solution (134 mM NaCl, 2.9 mM KCl, 2.1 mM $CaCl_2$, 1.2 mM $MgCl_2$, 10 mM HEPES, and 10 mM glucose, adjusted to pH 7.8 with NaOH) containing 150 mM tubocurarine was added. The agarose around the tail was removed using a surgical blade to allow efficient transfer of the drug solution. For high-speed voltage imaging, a fluorescence microscope (FN-1, Nikon) equipped with a CMOS camera (ORCA-Flash4.0, Hamamatsu Photonics) was used with a 40×/0.8 NA water-immersion lens. For most recordings, a 0.7× relay lens (NIKON) was also used. Fluorescence images were acquired using NIS-Elements (Nikon) software at approximately 16-200 Hz. High-speed confocal scanning was performed using a confocal microscope (Nikon A1R) with a 25×/1.0 NA water-immersion lens. For drug treatment, tetrodotoxin (1 μM, TOCRIS) was added to the extracellular solution using a peristaltic pump (World Precision Instruments). A thermo plate was used to keep the recording chamber at 28°C (Tokai hit).

Image analysis

133 Images were analyzed using the NIS-Elements (Nikon), Fiji, and OriginPro
134 (Lightstone) programs as described previously [41]. To extract changes in
135 fluorescence intensity, regions of interest (ROIs) were manually set using NIS-
136 element software (Nikon). Normalized changes in fluorescence intensity in the target
137 regions (ROIs) were quantitatively analyzed by calculating dF/F in the ROIs
138 ($dF/F_0=[F_{(t)}–F_0]/F_0$, where $F_{(t)}$ and F_0 are the fluorescence intensities at a certain
139 time point and initial time points, respectively). If the larvae/embryos moved during
140 the voltage imaging, the images were aligned using a Fiji program (TurboReg plugin).
141 Denoising and bleach corrections were also applied to some data using OriginPro
142 (Lightstone). Cross-correlation and hierarchical clustering analyses were performed
143 using OriginPro (Lightstone). The coupling rate was calculated as the ratio of the
144 frequency of target cell activity to that of mature cells. Among depolarizing signals
145 with small voltage changes, those characterized by a longer time to peak and a
146 shorter decay time were defined as "immature firing" and were distinguished from
147 other small depolarizations.
148
149 **Electrophysiological recordings**
150 Patch clamp recordings were conducted as described previously, using borosilicate
151 glass pipettes at 28 ℃ (World Precision Instrument, IB150F-4WPI) [24]. Electrical
152 responses were acquired via a Multiclamp 700B (Molecular devices) and DAQ
153 interface (National Instruments, USB-6212 BNC) with WinWCP software (Univ. of
154 Strathclyde), which also recorded the timing of image acquisition.
155
156
157 ## Results
158 **Establishment of voltage imaging using ArcLight zebrafish embryos**
159 To investigate voltage dynamics of neuronal populations in neuronal populations
160 during development, we established a transgenic zebrafish line that expresses
161 ArcLight specifically in neurons. We first established the transgenic line
162 Tg(*UAS:ArcLight*) using the GAL4-UAS and Tol2 transposon systems [37] (Fig. 1a).
163 To confirm ArcLight localization to cellular membranes in Tg(*UAS:ArcLight*) fish, we
164 examined Tg(*elavl3:GAL4-VP16;UAS:ArcLight;UAS:lyn-RFP*) embryos, in which
165 GAL4 is expressed in neurons and cellular membranes are labeled with Lyn-RFP.

166 At 1 dpf, ArcLight was widely observed in the neural tube and co-localized with Lyn-
167 RFP, indicating proper membrane localization of ArcLight in neurons (Fig. 1b, c).
168 Spinal cord neurons exhibit spontaneous firing early in development, with
169 coordinated activity of the neuronal populations beginning around 17 hpf [34, 43].
170 Consistent with this, Tg(*elavl3:GAL4-VP16;UAS:ArcLight*) embryos displayed
171 oscillatory changes in ArcLight fluorescence in the ventral spinal cord (Fig. 1d–g,
172 0.14±0.10 Hz, 6 fish). Fluorescence fluctuations alternated between the left and right
173 sides of the spinal cord, consistent with previous reports of periodic depolarization
174 (PD) in spinal neurons [43]. This activity was largely abolished following treatment
175 with the sodium channel blocker tetrodotoxin (TTX) (Fig. 1e-g). These results
176 demonstrate that ArcLight can reliably detect spontaneous activity in developing
177 spinal neurons.
178 We next examined whether ArcLight can resolve spinal voltage dynamics at
179 both single-cell and population levels. As shown in Figure 2, oscillatory activity was
180 clearly detected in individual neurons, with distinct amplitudes and temporal patterns
181 among neighboring neurons (Fig. 2a-c). Depolarizations typically propagated
182 sequentially along the rostrocaudal axis. In addition to large depolarizations that
183 closely resemble PD, small membrane potential fluctuations were also observed
184 between the PDs (Fig. 2d arrowheads). Based on their size and timing, these may
185 be synaptic bursts or subthreshold events, which are generally only captured by
186 electrophysiological recordings [43]. Cross-correlation analysis revealed strong
187 positive correlations among ipsilateral neurons and negative correlations between
188 contralateral pairs, indicating high synchrony within each side of the spinal cord (Fig.
189 2e). Hierarchical clustering analysis also supported this synchrony with partially
190 disordered activity along rostrocaudal axis (Fig. 2f). The depolarization was
191 confirmed by electrophysiological recordings (Supplementary Fig S1). To evaluate
192 the strength of ArcLight voltage imaging, we performed spinal calcium imaging using
193 Tg(*elavl3:GCaMP6f*) and compared its temporal resolution with ArcLight. Calcium
194 imaging exhibited substantially lower temporal resolution and reduced variability in
195 activity patterns (Supplementary Fig S1), highlighting the superior precision of the
196 GEVI ArcLight in capturing neural population dynamics.
197
198 **Subcellular voltage imaging of neural populations**

Measuring membrane potential dynamics in subcellular compartments such as axons and dendrites is crucial for understanding neuronal information processing [44, 45]. As shown in Figure 3, ArcLight voltage imaging successfully captured depolarizations in somata as well as in proximal and distal axonal regions. Although somata and axons exhibited similar depolarization patterns, the amplitude of voltage changes was slightly smaller in axons than in somata (Fig. 3b). Axonal depolarizations were also confirmed by confocal microscopy (Supplementary Fig. S2). Furthermore, high-resolution recordings revealed voltage fluctuations and morphological dynamics in fine structures such as filopodia (Supplementary Fig. S3).

Single-cell voltage imaging reveals simultaneous voltage and morphological dynamics

Spinal circuits comprise diverse neuronal types with distinct distributions, morphologies, and physiological properties [46]. To understand how these circuits develop, it is important to simultaneously monitor voltage dynamics and morphological changes. To achieve this, we used mosaic expression of ArcLight. By injecting *UAS-ArcLight* pDNA into Tg(*elavl3:GAL4-VP16*) fish, we sparsely labeled neurons, enabling high-resolution tracking of membrane potential changes and cellular morphology (Fig. 4a–c, 20 hpf, PMNs). We also captured voltage dynamics from interneurons that are otherwise difficult to identify (Fig. 4d, e). In addition to PD and synaptic burst (SB)-like activity, some neurons showed hyperpolarizing responses (Fig. 4e). Over the course of one hour, we observed notable morphological changes in these neurons, suggesting active developmental remodeling (Supplementary Fig. S4).

Developmental changes in voltage dynamics of neuronal populations

Finally, we investigated the emergence and maturation of voltage dynamics during development. Periodic firing in the spinal cord drives coiling behavior, analogous to fetal movement in humans, which are thought to contribute to spinal circuit formation [32]. This characteristic activity appears around 17 hpf and rapidly increases in frequency and amplitude until 20 hpf, followed by a gradual decline [34]. However, how population-level coordinated activity arises during this process remains to be elucidated.

To address this, we performed long-term voltage imaging of the spinal cord

along the course of development (Fig. 5). At 18 hpf, primary motor neurons (PMNs) possesses an axonal protrusion but seldom exhibited firing, instead showing small voltage fluctuations (Fig. 5c, arrowheads, cell 1, located at somite 8). These fluctuations were observed in both soma and axons (Supplementary Fig. S5) and displayed slower kinetics than mature firing (Supplementary Fig. S6). Over the next 30 minutes, PMNs gradually extended axons and increased firing frequency. By 19.5 hpf, the firing frequency reached ~0.3 Hz (0.29±0.05 Hz). In addition to cell 1, PMN cell 2, located more caudally, showed slower axonal extension and began firing after 18.5 hpf, ultimately synchronizing with other neurons by 19.5 hpf (Fig. 5). Similar temporal maturation patterns were also observed in other PMNs with some variability (Supplementary Fig. S7). Quantitative analyses revealed that firing frequency and coordination increased in tandem with axonal extension (Fig. 6a, b). In deede, the emergence of small depolarization and matured firing strongly correlated with morphological maturation (Fig. 6c, d). Moreover, coordination among PMNs also increased alongside the maturation of their individual voltage dynamics (Fig. 6e, f). These data suggest a sequence in the emergence of coordinated activity in spinal neurons: (1) absence of depolarization, (2) small depolarizations, (3) irregularly coordinated activity, and (4) fully synchronized firing.

To further assess how spontaneous activity evolves later in development, we extended voltage imaging to 23 hpf. By this stage, the previously regular and rapid firing observed at 20 hpf had decreased (Fig. 7, Supplementary Fig. S8). Depolarization patterns also changed—bursts became longer and left–right alternation diminished (Fig. 7b). Cross-correlation analysis revealed that at 20 hpf, neurons on both sides of the spinal cord were highly synchronized and exhibited strong periodicity (Fig. 7c). By 23 hpf, this coordination was largely diminished, although synchrony among ipsilateral neurons persisted. Notably, left–right alternating activity, which was prominent at 20–21 hpf, was markedly reduced at 23–24 hpf (Fig. 7d). These results suggest that while coordinated PMN activity declines during later stages of development, intra-hemispheric synchrony is maintained.

Discussion

Understanding how neuronal populations generate coordinated activity during development is a central challenge in neuroscience. Electrophysiological recordings have historically provided valuable insights into the membrane dynamics of spinal

neurons. However, these techniques are invasive and largely limited to short-duration and single-cell level [43, 46]. Calcium imaging has been used to examine developing circuits but lacks the temporal resolution and direct voltage sensitivity required to resolve fine membrane potential dynamics [42, 47, 48]. In this context, genetically encoded voltage indicators (GEVIs) offer a promising alternative, providing direct, fast, and non-invasive readouts of membrane potential. While GEVIs have been applied in mature brain tissues and cardiac tissues, their application to vertebrate embryonic development has remained rare due to technical limitations. To the best of our knowledge, this is the first study to achieve long-term voltage imaging of genetically defined neuronal populations in the spinal cord during development in a vertebrate model.

High-resolution imaging of voltage and morphological dynamics

Subcellular compartments—such as dendrites axons, and filopodia—play essential roles in neuronal function, shaping synaptic integration and signal propagation [44, 45]. In this study, ArcLight enabled voltage imaging not only at the soma, but also at proximal and distal axonal regions of primary motor neurons (PMNs). Notably, voltage fluctuations were also observed in filopodia, suggesting that even fine structures can exhibit membrane potential dynamics. Such fine-scale resolution opens opportunities to investigate the bioelectrical properties of neurite outgrowth, synaptogenesis, and structural remodeling. Combining voltage imaging with ratiometric or dual-color imaging approaches may allow simultaneous measurement of voltage and morphological parameters at high spatiotemporal precision [49].

Long-term population-level voltage dynamics in the developing spinal cord

The zebrafish spinal cord possesses one of the earliest neuronal circuits to form during development, and its transparency makes it an ideal model for in vivo imaging. Using a newly generated ArcLight transgenic line, we visualized voltage dynamics in spinal neuron populations from early developmental stages. At 20 hpf, we detected left-right alternating depolarizations, consistent with periodic depolarizations (PDs) previously observed via electrophysiology [34]. Compared to calcium imaging or earlier voltage sensors like ASAP1, ArcLight offered superior

temporal resolution and signal-to-noise ratio, respectively [13, 50]. This enabled detection of not only suprathreshold PDs, but also subthreshold events and hyperpolarizations, capturing a wider dynamic range of neuronal activity. Importantly, ArcLight could resolve activity patterns at both the single-cell and population levels, providing a comprehensive picture of how spinal circuits operate and evolve during development.

Emergence of voltage dynamics in the spinal neuron populations

One of the significant findings of this study is the stepwise emergence of coordinated voltage dynamics in motor neurons, closely tied to their morphological maturation. By performing long-term voltage imaging from, we found that PMNs followed a developmental sequence: (1) absence of depolarization, (2) emergence of small voltage fluctuations, (3) irregular and weakly coordinated activity, and (4) synchronized, robust left-right firing. This progression was strongly correlated with axonal extension, suggesting a tight coupling between structure and function.

It has been implicated that spinal cord neurons do not fire before axonal outgrowth, but detailed observation was missing [46]. Interestingly, here early voltage fluctuations preceded axon outgrowth, possibly driven by intrinsic dynamics of ion channels or electrical coupling via gap junctions, which predominate at these early stages. These small fluctuations may represent primitive forms of population synchrony, preceding the establishment of mature synaptic connections. This idea is consistent with other model systems where early electrical coupling plays an instructive role in circuit patterning [51].

Our approach provides a first-in-class demonstration of long-term, non-invasive voltage imaging in a developing vertebrate nervous system. Beyond the spinal cord, this approach can be extended to other regions, enabling a detailed dissection of diverse population dynamics during development. Furthermore, applying this imaging system to genetic models of neurodevelopmental disorders—such as autism spectrum disorders (ASD), epilepsy, or motor neuron disease—may allow the identification of early disruptions in coordinated neuronal activity. Detecting such early electrophysiological phenotypes could contribute to a better understanding of disease mechanisms.

In conclusion, we have established GEVI-based long-term voltage imaging

platform for long-term, high-resolution monitoring of developing neuronal populations in vivo. This system revealed the temporal emergence and maturation of population-level voltage dynamics in the spinal cord, offering new insights into how coordinated neural activity is built during development. The combination of spatial, temporal, and functional resolution achieved here represents a critical advance for the field of developmental neuroscience. By integrating this approach with optogenetics, cell-type-specific reporters, or functional perturbation, future studies can address how intrinsic and extrinsic factors shape circuit assembly. Moreover, our findings highlight the value of voltage imaging as a general tool for probing bioelectric mechanisms in morphogenesis, circuit development, and disease [52, 53].

Acknowledgement

We thank Drs Koichi Kawakami, Shinichi Higashijima, Hitoshi Okamoto, Hisashi Kakinuma, and Ryunosuke Amo for providing fish lines; Kyo Yamasu for plasmid DNA; Junichi Nakai, Masamichi Ohkura, and Keiko Ando for technical support; and Lawrence Cohen and Shinichi Higashijima for helpful discussions. This work was supported in part by JSPS KAKENHI (Grants-in-Aid for Scientific Research), JST Tenure Track program at Saitama University (SUTT), Strategic Research Program for Brain Science from Ministry of Education, Culture, Sports, JST A-STEP Grant Number JPMJTM20C05, New Energy and Industrial Technology Development Organization (NEDO), Kao Foundation grant, Asahi Glass Foundation, and Kato-bio Foundation.

Author Contributions

A.S, A.H., N.F., M.H., K.M., and S.T. performed the experiments. S.T. conceived and designed the experiments. S.T., A.S., A.H., and N.F. wrote the manuscript. All authors reviewed the manuscript.

Competing interests

The authors declare no competing interests.

References

1. Cohen, L.B. and B.M. Salzberg, *Optical measurement of membrane potential.* Rev Physiol Biochem Pharmacol, 1978. **83**: p. 35-88.
2. Loew, L.M., et al., *Evidence for a charge-shift electrochromic mechanism in a probe of membrane potential.* Nature, 1979. **281**(5731): p. 497-9.
3. Djurisic, M., et al., *Optical monitoring of neural activity using voltage-sensitive dyes.* Methods Enzymol, 2003. **361**: p. 423-51.
4. Lin, M.Z. and M.J. Schnitzer, *Genetically encoded indicators of neuronal activity.* Nat Neurosci, 2016. **19**(9): p. 1142-53.
5. Homma, R., et al., *Wide-field and two-photon imaging of brain activity with voltage- and calcium-sensitive dyes.* Philos Trans R Soc Lond B Biol Sci, 2009. **364**(1529): p. 2453-67.
6. Yan, P., et al., *Palette of fluorinated voltage-sensitive hemicyanine dyes.* Proc Natl Acad Sci U S A, 2012. **109**(50): p. 20443-8.
7. Wuskell, J.P., et al., *Synthesis, spectra, delivery and potentiometric responses of new styryl dyes with extended spectral ranges.* J Neurosci Methods, 2006. **151**(2): p. 200-15.
8. Momose-Sato, Y., T. Nakamori, and K. Sato, *Spontaneous depolarization wave in the mouse embryo: origin and large-scale propagation over the CNS identified with voltage-sensitive dye imaging.* Eur J Neurosci, 2012. **35**(8): p. 1230-41.
9. Rokni, D., R. Llinas, and Y. Yarom, *Stars and stripes in the cerebellar cortex: a voltage sensitive dye study.* Front Syst Neurosci, 2007. **1**: p. 1.
10. Roome, C.J. and B. Kuhn, *Dendritic coincidence detection in Purkinje neurons of awake mice.* Elife, 2020. **9**.
11. Storace, D., et al., *Toward Better Genetically Encoded Sensors of Membrane Potential.* Trends Neurosci, 2016. **39**(5): p. 277-289.
12. Kannan, M., G. Vasan, and V.A. Pieribone, *Optimizing Strategies for Developing Genetically Encoded Voltage Indicators.* Front Cell Neurosci, 2019. **13**: p. 53.
13. Bando, Y., et al., *Comparative Evaluation of Genetically Encoded Voltage Indicators.* Cell Rep, 2019. **26**(3): p. 802-813 e4.
14. Akemann, W., et al., *Imaging neural circuit dynamics with a voltage-sensitive fluorescent protein.* J Neurophysiol, 2012. **108**(8): p. 2323-37.
15. Jin, L., et al., *Single action potentials and subthreshold electrical events imaged in neurons with a fluorescent protein voltage probe.* Neuron, 2012. **75**(5): p. 779-85.
16. St-Pierre, F., et al., *High-fidelity optical reporting of neuronal electrical activity with an ultrafast fluorescent voltage sensor.* Nat Neurosci, 2014. **17**(6): p. 884-9.
17. Tsutsui, H., et al., *Improving membrane voltage measurements using FRET with new fluorescent proteins.* Nat Methods, 2008. **5**(8): p. 683-5.

18. Hochbaum, D.R., et al., *All-optical electrophysiology in mammalian neurons using engineered microbial rhodopsins.* Nat Methods, 2014. **11**(8): p. 825-33.
19. Gong, Y., et al., *High-speed recording of neural spikes in awake mice and flies with a fluorescent voltage sensor.* Science, 2015. **350**(6266): p. 1361-6.
20. Abdelfattah, A.S., et al., *Bright and photostable chemigenetic indicators for extended in vivo voltage imaging.* Science, 2019. **365**(6454): p. 699-704.
21. Piatkevich, K.D., et al., *A robotic multidimensional directed evolution approach applied to fluorescent voltage reporters.* Nat Chem Biol, 2018. **14**(4): p. 352-360.
22. Nakajima, R. and B.J. Baker, *Mapping of excitatory and inhibitory postsynaptic potentials of neuronal populations in hippocampal slices using the GEVI, ArcLight.* J Phys D Appl Phys, 2018. **51**(50).
23. Storace, D.A. and L.B. Cohen, *Measuring the olfactory bulb input-output transformation reveals a contribution to the perception of odorant concentration invariance.* Nat Commun, 2017. **8**(1): p. 81.
24. Miyazawa, H., et al., *Optical interrogation of neuronal circuitry in zebrafish using genetically encoded voltage indicators.* Sci Rep, 2018. **8**(1): p. 6048.
25. Bohm, U.L., et al., *Voltage imaging identifies spinal circuits that modulate locomotor adaptation in zebrafish.* Neuron, 2022. **110**(7): p. 1211-1222 e4.
26. Yang, H.H., et al., *Subcellular Imaging of Voltage and Calcium Signals Reveals Neural Processing In Vivo.* Cell, 2016. **166**(1): p. 245-57.
27. Jia, B.Z., et al., *A bioelectrical phase transition patterns the first vertebrate heartbeats.* Nature, 2023. **622**(7981): p. 149-155.
28. Yoshimatsu, T., et al., *Ancestral circuits for vertebrate color vision emerge at the first retinal synapse.* Sci Adv, 2021. **7**(42): p. eabj6815.
29. Lu, X., et al., *Widefield imaging of rapid pan-cortical voltage dynamics with an indicator evolved for one-photon microscopy.* Nat Commun, 2023. **14**(1): p. 6423.
30. Grillner, S., *Neurobiological bases of rhythmic motor acts in vertebrates.* Science, 1985. **228**(4696): p. 143-9.
31. McLean, D.L., et al., *A topographic map of recruitment in spinal cord.* Nature, 2007. **446**(7131): p. 71-5.
32. Menelaou, E., et al., *Embryonic motor activity and implications for regulating motoneuron axonal pathfinding in zebrafish.* Eur J Neurosci, 2008. **28**(6): p. 1080-96.
33. Fidelin, K. and C. Wyart, *Inhibition and motor control in the developing zebrafish spinal cord.* Curr Opin Neurobiol, 2014. **26C**: p. 103-109.
34. Saint-Amant, L., *Development of motor rhythms in zebrafish embryos.* Prog Brain Res, 2010. **187**: p. 47-61.
35. O'Donovan, M.J., *The origin of spontaneous activity in developing networks of the vertebrate nervous system.* Curr Opin Neurobiol, 1999. **9**(1): p. 94-104.

36. Ahrens, M.B., et al., *Brain-wide neuronal dynamics during motor adaptation in zebrafish.* Nature, 2012. **485**(7399): p. 471-7.
37. Asakawa, K., et al., *Genetic dissection of neural circuits by Tol2 transposon-mediated Gal4 gene and enhancer trapping in zebrafish.* Proc Natl Acad Sci U S A, 2008. **105**(4): p. 1255-60.
38. Lister, J.A., et al., *nacre encodes a zebrafish microphthalmia-related protein that regulates neural-crest-derived pigment cell fate.* Development, 1999. **126**(17): p. 3757-67.
39. Kimura, Y., C. Satou, and S. Higashijima, *V2a and V2b neurons are generated by the final divisions of pair-producing progenitors in the zebrafish spinal cord.* Development, 2008. **135**(18): p. 3001-5.
40. Nakayama, Y., et al., *Comprehensive analysis of target genes in zebrafish embryos reveals gbx2 involvement in neurogenesis.* Dev Biol, 2017. **430**(1): p. 237-248.
41. Hiyoshi, K., et al., *In vivo wide-field voltage imaging in zebrafish with voltage-sensitive dye and genetically encoded voltage indicator.* Dev Growth Differ, 2021. **63**(8): p. 417-428.
42. Muto, A., et al., *Genetic visualization with an improved GCaMP calcium indicator reveals spatiotemporal activation of the spinal motor neurons in zebrafish.* Proc Natl Acad Sci U S A, 2011. **108**(13): p. 5425-30.
43. Saint-Amant, L. and P. Drapeau, *Motoneuron activity patterns related to the earliest behavior of the zebrafish embryo.* J Neurosci, 2000. **20**(11): p. 3964-72.
44. London, M. and M. Hausser, *Dendritic computation.* Annu Rev Neurosci, 2005. **28**: p. 503-32.
45. Garrido, J.J., et al., *Dynamic compartmentalization of the voltage-gated sodium channels in axons.* Biol Cell, 2003. **95**(7): p. 437-45.
46. Saint-Amant, L. and P. Drapeau, *Synchronization of an embryonic network of identified spinal interneurons solely by electrical coupling.* Neuron, 2001. **31**(6): p. 1035-46.
47. Wan, Y., et al., *Single-Cell Reconstruction of Emerging Population Activity in an Entire Developing Circuit.* Cell, 2019. **179**(2): p. 355-372 e23.
48. Warp, E., et al., *Emergence of patterned activity in the developing zebrafish spinal cord.* Curr Biol, 2012. **22**(2): p. 93-102.
49. Kim, B.B., et al., *A red fluorescent protein with improved monomericity enables ratiometric voltage imaging with ASAP3.* Sci Rep, 2022. **12**(1): p. 3678.
50. Storace, D.A., et al., *Monitoring brain activity with protein voltage and calcium sensors.* Sci Rep, 2015. **5**: p. 10212.
51. Gutierrez, G.J., T. O'Leary, and E. Marder, *Multiple mechanisms switch an electrically coupled, synaptically inhibited neuron between competing rhythmic oscillators.* Neuron, 2013. **77**(5): p. 845-58.

485 # Figure Legends

486 **Figure 1**

487 Transgenic zebrafish showing membrane-localized ArcLight and spontaneous
488 activity in the neural tube. (a) Schematic diagram of plasmid construct for ArcLight.
489 (b) Lateral views of ArcLight-expressing embryos at 1 dpf. ArcLight is distributed
490 widely in the neural tube of Tg*(elavl3:GAL4-VP16;UAS:ArcLight)* fish. (c) Dorsal
491 view of the neural tube of Tg*(elavl3:GAL4-VP16;UAS:ArcLight;UAS:lyn-RFP)*
492 embryos at 1 dpf. ArcLight (green) is co-localized with Lyn-RFP (red: cell
493 membranes) in the neural tube (arrowheads). Higher magnification images are
494 shown in the lower panel. (d-f) Spontaneous activity of spinal cord neurons is
495 detected by ArcLight imaging. (d) Dorsal view of the ventral spinal cord of Tg
496 *(elavl3:GAL4-VP16;UAS:ArcLight-A242)* fish at 20 hpf. The rostral side is to the left,
497 and the area between 3–8 somites is shown. A schematic diagram of the imaging
498 system is shown on the right. Changes in the fluorescence of ArcLight ($-\Delta F/F_0$) are
499 indicated by the pseudocolor scale shown at right. White arrowheads indicate the
500 activated neurons. Regions of interest (ROIs) located between 5–7 somites are
501 indicated by red (right side) and blue (left side) rectangular in (d). Fluorescence
502 changes of ArcLight in the ROIs are shown on the right. The time point of the image
503 is indicated by a black arrowhead. (f-g) The spontaneous activity in the spinal cord
504 mostly disappeared by tetrodotoxin (TTX) treatment (control 0.14±0.10 Hz, TTX
505 0.01±0.02 Hz, $p<0.05$, right side: control 0.14±0.10 Hz, TTX 0.01±0.02 Hz, *: $p<0.05$,
506 Wilcoxon signed-rank test, 6 fish). The imaged plane and ROIs are in the same
507 positions as in (d).

508

509 **Figure 2**

510 Monitoring spontaneous activity of individual cells in the spinal cord by ArcLight
511 imaging. (a) A fluorescence image of the ventral spinal cord of Tg*(elavl3:GAL4-*
512 *VP16;UAS:ArcLight)* fish at 21 hpf. ROIs are located at the 18 cells (red: right side,
513 blue: left side). Higher magnification views are shown on the right. (b) Changes in
514 ArcLight signal at the two time points indicated in (c). (c) Activity patterns of the 18
515 cells are shown. Higher magnification views of the ArcLight signal of cells 4 and 13
516 are shown at the bottom. (d). (e, f) Hierarchal clustering analysis of the voltage
517 dynamics in the 18 cells shows the synchronous activity in the ipsilateral neuron
518 pairs (e), and also several groups with higher synchrony within them (f).

Figure 3

Voltage imaging of spinal cord neurons at a high spatiotemporal resolution at the cellular compartment level by ArcLight. (a) Lateral views of the spinal cord of Tg*(elavl3:GAL4-VP16;UAS:ArcLight)* fish at 20 hpf. A schematic diagram of the imaging system is shown on the right. (b) Changes in ArcLight signal are observed at soma and axons in three different ROIs shown in (a). Higher resolution observations are shown in Supplementary Fig. S2 and S3.

Figure 4

Single cell labeling of neurons by ArcLight enables simultaneous recording of voltage and morphology. (a) Schematic diagram of the co-injection experiment. (b) A stacked confocal image of the spinal cord region of the injected embryo at 20 hpf. The left side view is shown. Arrowheads and arrows indicate the soma and axons of ArcLight positive cells, respectively. (c) Voltage dynamics of a primary motor neuron are indicated by a yellow arrowhead in (b). ROIs at soma and axons are shown in red and blue, respectively. (d, e) Voltage imaging of the spinal cord interneurons. A higher magnification view is shown in (e). ArcLight signals from three cells are shown on the right. In addition to periodic depolarization, hyperpolarization (white arrowheads) and subthreshold-like signals (black arrowheads) are observed.

Figure 5

Long-term voltage imaging of the spinal cord PMNs shows the emergence of population activity. (a) Left views of the spinal cord of ArcLight positive fish from 18 hpf to 19.5 hpf. (b) Enlarged views of (a). (c) Voltage dynamics obtained from the axons of the two cells shown in (a). Black and white arrowheads indicate small depolarization and immature firing, respectively.

Figure 6

Characteristic patterns of depolarization observed during the development of PMNs population activity. Quantitative analysis indicates that coupled activity among PMNs emerged via small depolarization and immature firing. (a,b) (a) The relationship between axon length and firing frequency. (b) The relationship between

552 axon length and coordination with neighboring neurons. Developmental process of
553 each PMN is indicated by lines. Developmental stages are indicated by dots colors.
554 (c) The relationship between the axonal length and existence of small depolarization
555 (no depolarization: 13.76±3.75 μm, small depolarization: 11.97±1.67 μm, Firing:
556 27.12±1.38 μm, 5 fish, 30 cells, **p<0.01, Mann–Whitney U test). (d) The
557 relationship between axonal length and immature firings (no depolarization:
558 10.48±2.38 μm, small depolarization: 22.42±2.69 μm, Firing: 26.06±1.44 μm, 5 fish,
559 30 cells, **p<0.01, Mann–Whitney U test). (e) Comparison of coupling rates between
560 PMNs with small depolarizations and those with firings (immature and mature firings)
561 (small depolarization: 0.24±0.07, firing: 0.93±0.03, 4 fish, 18 cells,, **p<0.01, Mann–
562 Whitney U test). (f) Comparison of coupling rates between PMNs exhibiting immature
563 and mature firings (immature firing: 0.58±0.10, mature firing: 0.94±0.03, 4 fish, 18
564 cells, **p<0.01, Mann–Whitney U test).
565
566 **Figure 7**
567 Changes in firing properties in spinal cord neuron populations. (a) Dorsal view of
568 ArcLight positive spinal cord at 20 hpf. (b) Voltage dynamics of each neuron are
569 shown at 20 and 23 hpf. The position of ROIs is indicated in (a). (c) Cross-correlation
570 analysis of ipsilateral and contralateral pairs of spinal cord neurons at 20 and 23 hpf.
571 (d) Probability of altering activity at 23-24 hpf was significantly reduced compared
572 to that at 23-24 hpf. 20–21 hpf: 98.9±1.10%; 23–24 hpf: 98.9±1.10%, 5 fish; 23–24
573 hpf: 79.8%±5.71%, 4 fish; p<0.05, Mann–Whitney U test.
574
575 **Supplementary Figure S1**
576 Monitoring spontaneous activity of individual cells in the spinal cord by calcium
577 imaging by GCaMP6f. (a) Fluorescence image of the ventral spinal cord of
578 Tg*(elavl3: GCaMP6f)* embryo at 21 hpf. ROIs were placed on six cells (red: right
579 side, blue: left side). Higher-magnification views are shown on the right. (b)
580 Schematic diagram of the recording setup. (c) Activity patterns of the six cells shown
581 in (a). (d) A higher magnification view of the ArcLight signal of cells 1 and 5. (e)
582 Simultaneous recordings of membrane potential by cell-attached patch-clamp
583 recordings and ArcLight imaging showed that the recorded neurons were indeed
584 depolarized. A fluorescence image of the spinal cord of Tg*(HuC:GVP;UAS:ArcLight)*

585 fish at 23 hpf. (f) Voltage (top) and optical (bottom) signals detected at the cell
586 indicated in (e).
587
588 **Supplementary Figure S2**
589 Confocal observation of ArcLight expression and voltage dynamics in the spinal cord.
590 (a) Lateral views of Tg*(elavl3:GAL4-VP16;UAS:ArcLight)* embryo at 1 dpf. Higher
591 magnification images shown on the right indicate filopodia and lamellipodia of
592 primary motor neurons (arrowheads). (b) Voltage imaging of cell1 in (a). ROIs were
593 set at the axonal region. ArcLight detected depolarization at axons (black
594 arrowheads). The gray area is the period when the embryos moved.
595
596 **Supplementary Figure S3**
597 Voltage imaging of a primary motor neuron at higher spatial resolution. (a) Left views
598 of the spinal cord at two different time points. Arrowheads indicate filopodia (white,
599 yellow). A yellow arrowhead indicates a filopodium that shows a prominent extension.
600 (b, c) An example of voltage dynamics detected at various positions in the axon.
601 ROI4-6 were set on a filopodium. ROI 7 was set in a region where no clear structure
602 was observed.
603
604 **Supplementary Figure S4**
605 Single-cell labeling by ArcLight shows the morphological changes of the spinal cord
606 neurons. Images taken at 21 hpf and 22 hpf are shown. An arrowhead indicates a
607 growth cone of the extending axon.
608
609 **Supplementary Figure S5**
610 Developmental changes in the voltage dynamics of PMNs at the soma and axons.
611 Voltage dynamics were generally similar between the soma and axons.
612 Representative traces from Cell 2 in Figure 5 are shown.
613
614 **Supplementary Figure S6**
615 Comparison of voltage dynamics between immature and mature firings. Immature
616 firings showed a significantly longer time to peak (a) but not decay time (b) (time to
617 peak; immature firing: 1.31±0.43 s, mature firing: 0.63±0.20 s, decay time; immature

618 firing: 0.59±0.25 s, mature firing: 0.50±0.17 s, **p < 0.01, Mann–Whitney U test, 3
619 fish, 65 transients).
620
621 **Supplementary Figure S7**
622 Developmental change in the voltage dynamics of PMNs. (a-e) Left-side views of
623 the spinal cord of ArcLight-positive fish from 18 to 20 hpf (top), and corresponding
624 voltage traces (bottom) of the PMNs indicated by arrowheads. ROIs were set on
625 axons, as shown in (f).
626
627 **Supplementary Figure S8**
628 Long-term voltage imaging shows the changes in the firing patterns of the spinal
629 cord neurons population. (a) ROIs position of cells 1-6. (b) Voltage dynamics of the
630 6 cells are shown from 20 to 23 hpf. Cells on the right and left sides of the spinal
631 cord are shown in red and blue, respectively.
632
633 **Supplementary Movie1**
634 Spontaneous activity of individual cells in the spinal cord is observed by ArcLight.
635 Dorsal view of the ventral spinal cord of Tg*(elavl3:GAL4-VP16;UAS:ArcLight)* fish at
636 21 hpf.
637
638 **Supplementary Movie2**
639 Monitoring of spontaneous activity of spinal cord neurons, including primary motor
640 neurons by ArcLight. Left view of the spinal cord of Tg*(elavl3:GAL4-*
641 *VP16;UAS:ArcLight)* fish at 20 hpf.
642
643 **Supplementary Movie3**
644 Single-cell labeling and voltage imaging of spinal cord neurons using ArcLight. Left
645 view of the spinal cord of Tg*(elavl3:GAL4-VP16)* embryo at 21 hpf. A high-resolution
646 image is shown in Supplementary Figure S4.
647
648 **Supplementary Movie4**
649 Voltage dynamics of an axonal region of a primary motor neuron at a high spatial
650 resolution. Left view of the spinal cord Tg*(elavl3:GAL4-VP16;UAS:ArcLight)* fish at

18.5 hpf.

Supplementary Movie5

Voltage imaging of spinal neurons at 18.5 hpf (12 s). Left-side view is shown.

Supplementary Movie6

Voltage imaging of spinal neurons at 19 hpf (12 s). Left-side view is shown.

Supplementary Movie7

Voltage imaging of spinal neurons at 19.5 hpf (12 s). Left-side view is shown.

Figure 1

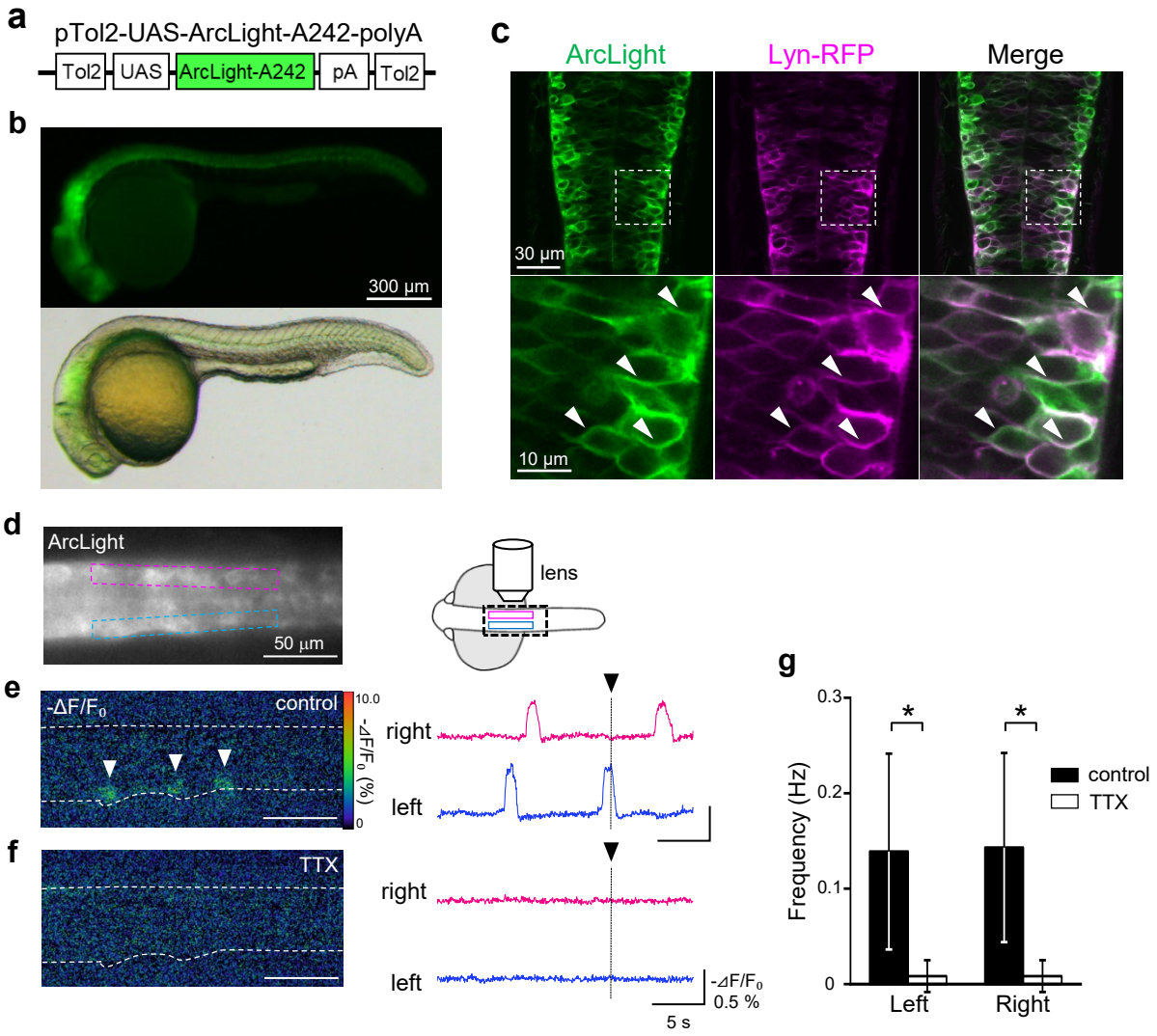
a
pTol2-UAS-ArcLight-A242-polyA
Tol2
UAS
ArcLight-A242
pA
Tol2
b
300 μm
c
ArcLight
Lyn-RFP
Merge
30 μm
10 μm
d
ArcLight
50 μm
lens
e
-ΔF/F0
control
10.0
-ΔF/F0 (%)
0
f
TTX
right
left
right
left
-ΔF/F0
0.5 %
5 s
g
0.3
0.2
0.1
0
Frequency (Hz)
*
*
control
TTX
Left
Right

Figure 2

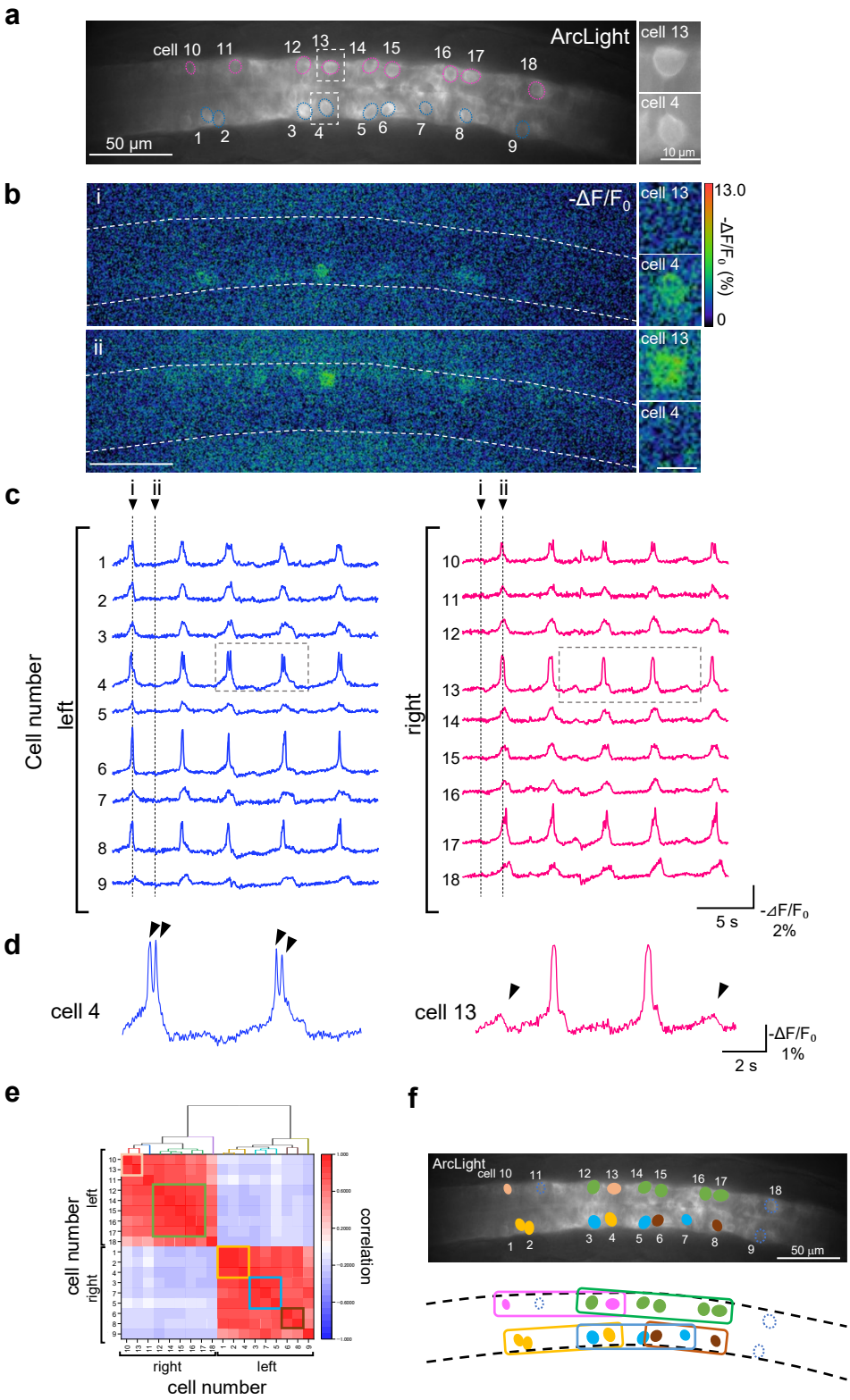
a
ArcLight
cell 10
11
12
13
14
15
16
17
18
1
2
3
4
5
6
7
8
9
50 µm
cell 13
cell 4
10 µm
b
i
ii
-ΔF/F0
cell 13
cell 4
13.0
-ΔF/F0 (%)
0
c
Cell number
left
right
5 s
-ΔF/F0
2%
d
cell 4
cell 13
2 s
-ΔF/F0
1%
e
cell number
left
right
correlation
f
ArcLight
50 µm

Figure 3

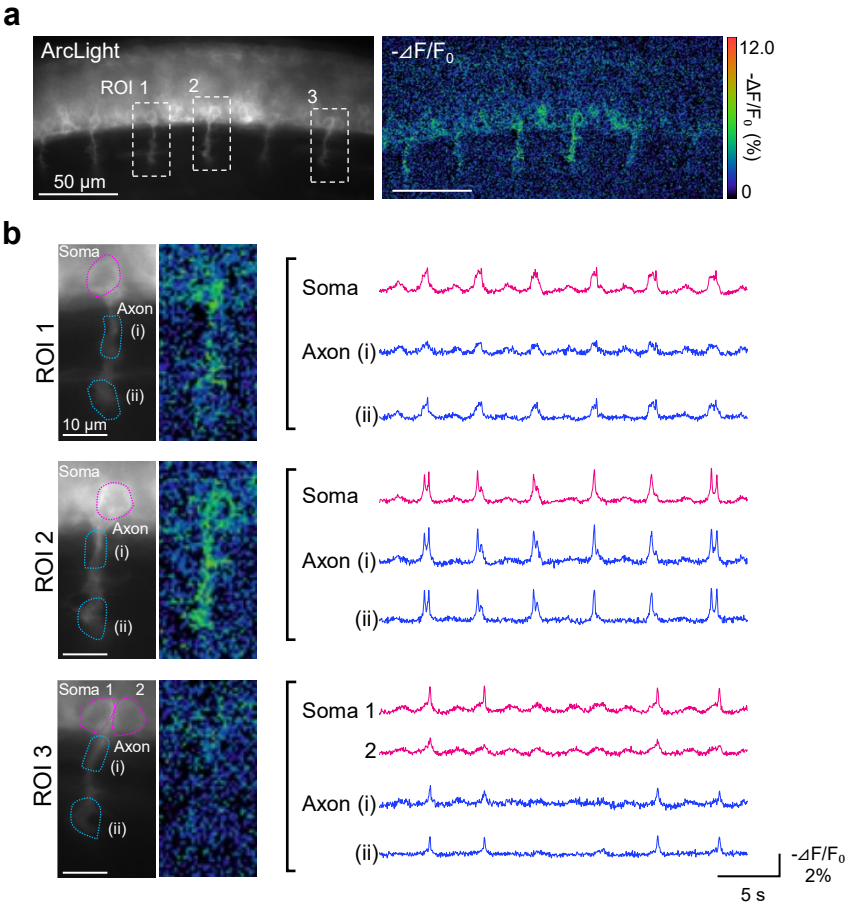
a
ArcLight
ROI 1
2
3
50 μm
-⊿F/F0
12.0
-ΔF/F0 (%)
0
b
ROI 1
Soma
Axon
(i)
(ii)
10 μm
Soma
Axon (i)
(ii)
ROI 2
Soma
Axon
(i)
(ii)
Soma
Axon (i)
(ii)
ROI 3
Soma 1
2
Axon
(i)
(ii)
Soma 1
2
Axon (i)
(ii)
-⊿F/F0
2%
5 s

Figure 4

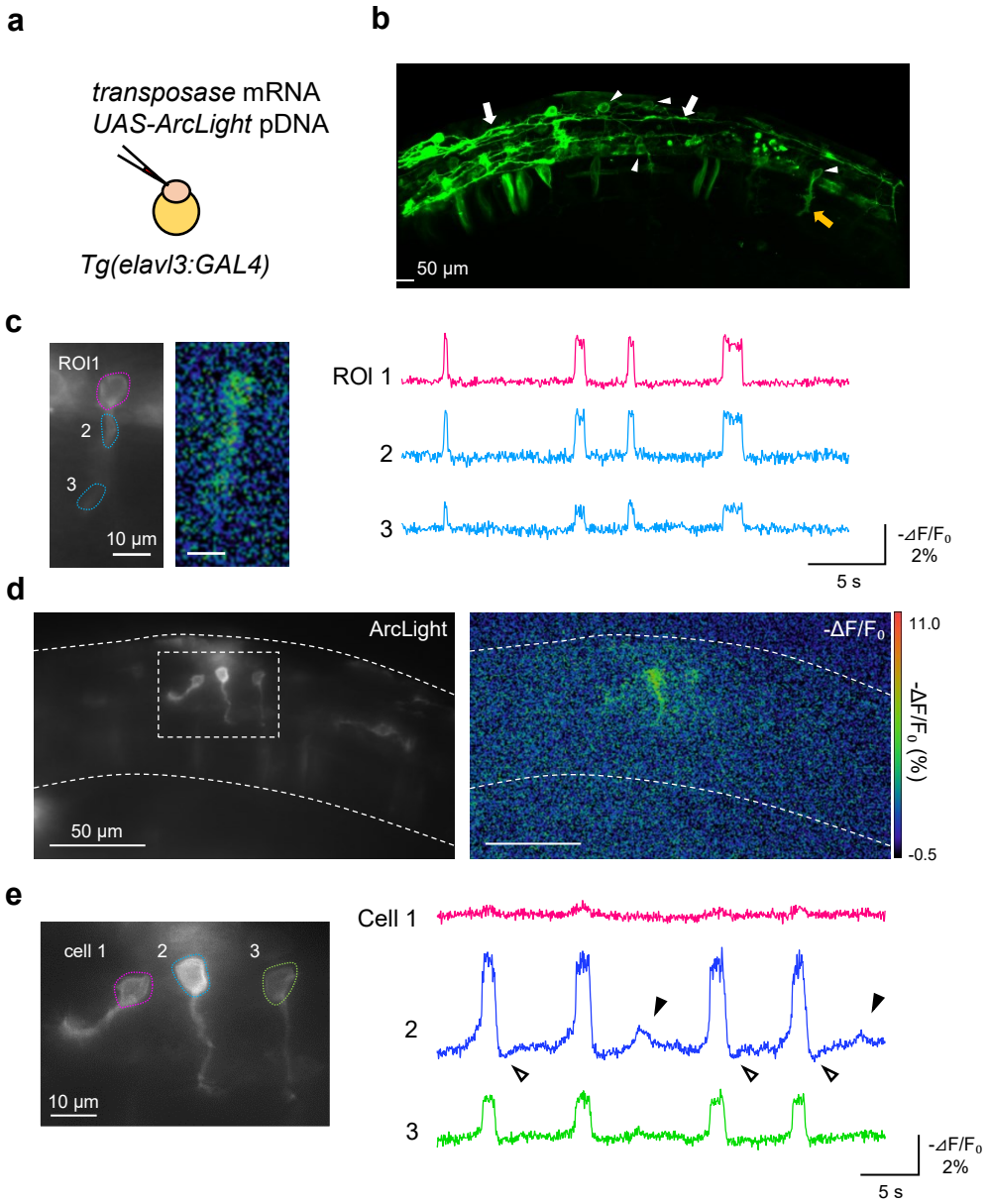
a
transposase mRNA
UAS-ArcLight pDNA
Tg(elavl3:GAL4)
b
50 μm
c
ROI1
2
3
10 μm
ROI 1
2
3
-ΔF/F0
2%
5 s
d
ArcLight
50 μm
-ΔF/F0
11.0
-ΔF/F0 (%)
-0.5
e
cell 1
2
3
10 μm
Cell 1
2
3
-ΔF/F0
2%
5 s

Figure 5

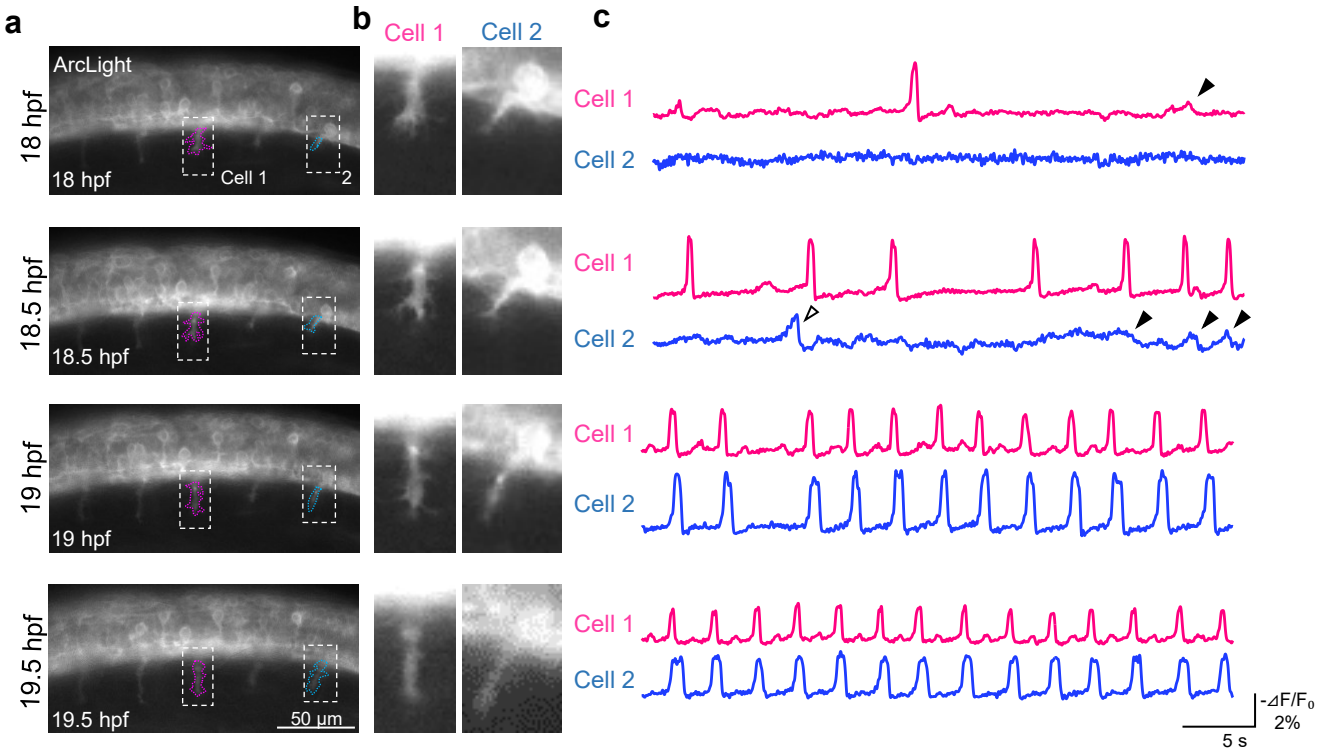
a
b
c
Cell 1
Cell 2
ArcLight
18 hpf
18.5 hpf
19 hpf
19.5 hpf
Cell 1
2
50 µm
-ΔF/F0
2%
5 s

Figure 6

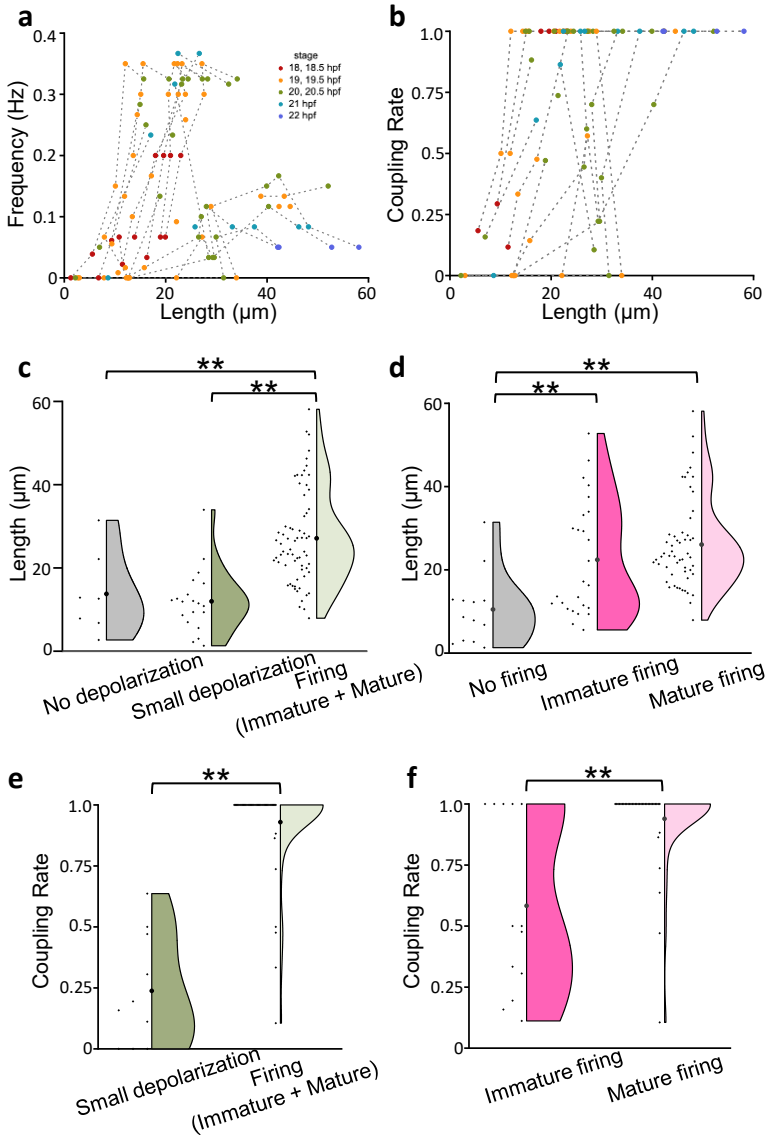
a
Frequency (Hz)
Length (µm)
stage
18, 18.5 hpf
19, 19.5 hpf
20, 20.5 hpf
21 hpf
22 hpf
b
Coupling Rate
Length (µm)
c
Length (µm)
**
**
No depolarization
Small depolarization
Firing
(Immature + Mature)
d
Length (µm)
**
**
No firing
Immature firing
Mature firing
e
Coupling Rate
**
Small depolarization
Firing
(Immature + Mature)
f
Coupling Rate
**
Immature firing
Mature firing

Figure 7

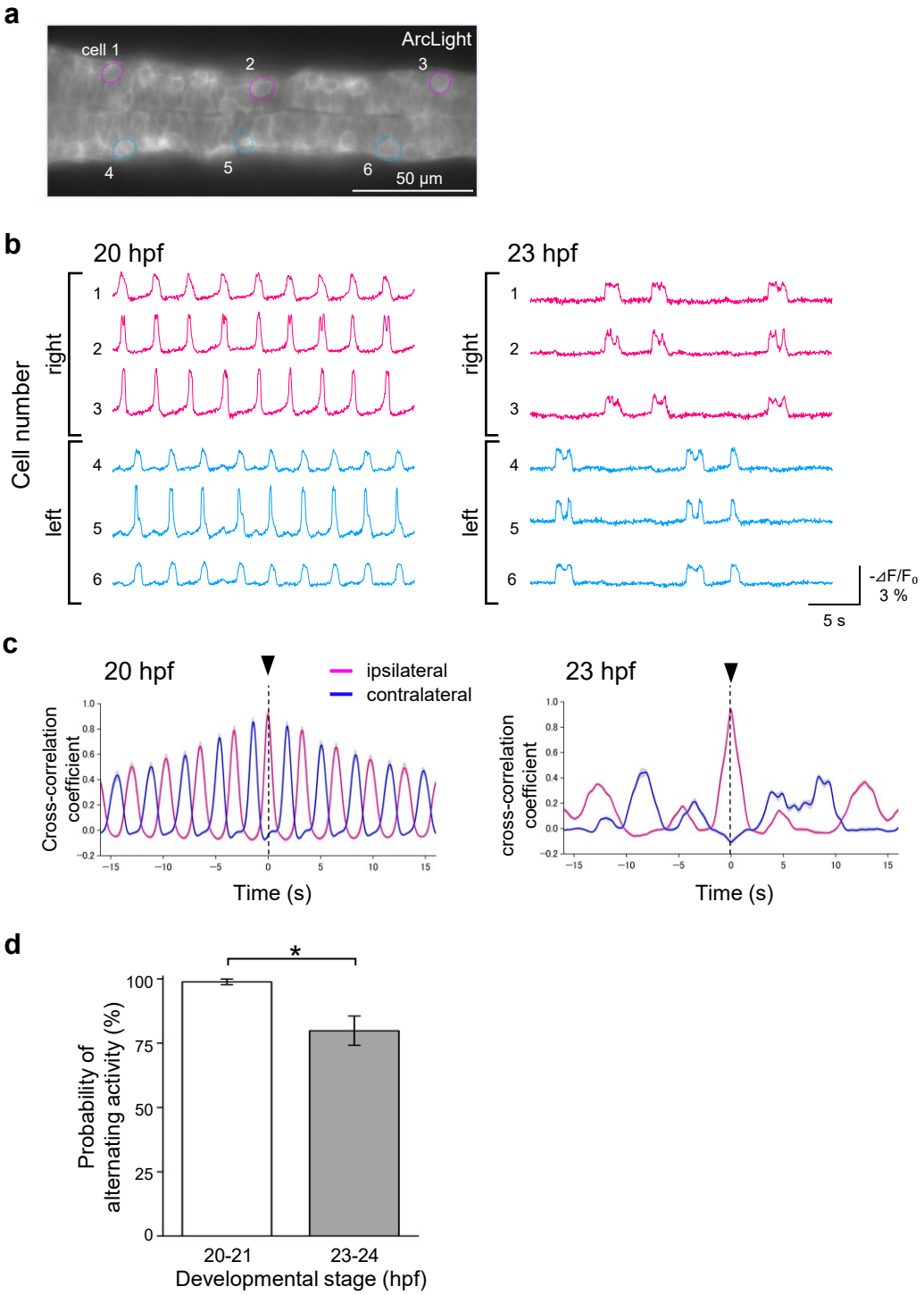
a
cell 1
2
3
ArcLight
4
5
6
50 µm
b
20 hpf
23 hpf
Cell number
right
left
1
2
3
4
5
6
-ΔF/F0
3 %
5 s
c
20 hpf
23 hpf
ipsilateral
contralateral
Cross-correlation coefficient
cross-correlation coefficient
Time (s)
d
*
Probability of alternating activity (%)
100
75
50
25
0
20-21
23-24
Developmental stage (hpf)